EFFECT OF TEMPERATURE AND SOLAR IRRADIANCE ON THE PERFORMANCE OF 50 HZ PHOTOVOLTAIC WIRELESS POWER TRANSFER SYSTEM

M. Irwanto[a,b]*, Y. T. Nugraha[a], N. Hussin[b], I. Nisja[c]

[a]Department of Electrical Engineering, Universitas Prima Indonesia (UNPRI), Medan, Indonesia
[b]Fellow of Center of Excellence for Renewable Energy (CERE), Universiti Malaysia Perlis (UniMAP), Perlis, Malaysia
[c]Department of Electrical Engineering, Universitas Bung Hatta (UBH), Padang, Indonesia

Graphical abstract

Abstract

The previous researchers on wireless power transfer (WPT) systems were able to transmit the AC power, although their AC frequencies were high in some kilohertz or megahertz. They were unable to be applied directly on the AC loads or only administered to the DC energy after rectification through a rectifier circuit. In the receiver phase, the AC power was also very low, due to the minimum voltage and current on the receiver coil (RC). Therefore, this study aims to determine the effects of temperature and solar irradiance on the performance of the 50 Hz photovoltaic wireless power transfer (PVWPT) system. It is constructed by some PV modules in series connection, to achieve a required DC voltage level on the DC-DC converter and receiver phase. It also converts DC to AC voltages on the transmitter coil (TC) of an H-bridge inverter, with a receiver circuit and a magnetic relay coil positioned between the TC and RC. The results showed that solar irradiance and temperature affected the performances of the PV module and PVWPT system. This indicated that higher solar irradiance increased the performance of the PVWPT system, whose maximum efficiency was achieved by positioning the magnetic relay coil between the TC and RC. At the solar irradiance and temperature of 100 W/m2 and 26°C, the lowest value of PVWPT efficiency was 47.92%. Meanwhile, the highest value was 48.1% at 1000 W/m2 and 29°C. This proved that the efficiency of the PVWPT system ranged from 47.92-48.1%, with its average value being 48%.

Keywords: Temperature, Solar irradiance, Photovoltaic, Wireless power transfer, Magnetic relay coil

Abstrak

Penyelidikan sistem pemindahan kuasa tanpa wayar (KTW) sebelum ini telah berjaya menghantar kuasa AU, tetapi frekuensi AU adalah frekuensi tinggi dalam beberapa kilohertz atau megahertz. Ia hanya boleh digunakan pada tenaga AT selepas diteruskan oleh litar penerus, atau ia tidak boleh digunakan pada beban AU secara langsung. Juga, kuasa AU pada bahagian penerima adalah sangat rendah, ia disebabkan oleh voltan rendah dan arus pada gegelung penerima (RC). Kertas kerja ini membentangkan simulasi sistem pemindahan 50 Hz fotovoltaik (PV) kuasa tanpa wayar (KTW). Ia dibina oleh beberapa modul PV dalam sambungan bersiri untuk mencapai tahap voltan AT yang diperlukan pada bahagian penukar AT-AT dan sisi penerima. Ia juga menukar voltan AT menjadi voltan AU pada gegelung pemancar (TC) dari satu penyongsang jambatan-H, litar penerima dan gegelung geganti magnet yang diletakkan di antara TC dan RC. Hasil simulasi menunjukkan bahawa sinaran suria dan suhu mempengaruhi prestasi modul PV dan sistem PVKTW. Peningkatan sinaran suria akan meningkatkan prestasi sistem PVKTW. Prestasi sistem

PVKTW yang lebih tinggi boleh dicapai dengan meletakkan gegelung geganti magnet antara gegelung pemancar dan penerima. Pada sinaran suria dan suhu 100 W/m² dan 26°C, nilai kecekapan PVWPT terendah ialah 47.92%. Manakala, nilai tertinggi ialah 48.1% pada 1000 W/m² dan 29°C. Ini membuktikan bahawa kecekapan sistem PVWPT adalah antara 47.92-48.1%, dengan nilai puratanya ialah 48%.

Kata kunci: Suhu, Sinaran suria, Fotovoltaik, Pemindahan kuasa tanpa wayar, Gegelung geganti magnet

1.0 INTRODUCTION

Solar radiation is a sun fusion process that produces and emits energy to the surface of the earth. This radiation is divided into two parts, namely (1) solar irradiance, the sun power density with a unit of W/m², and (2) solar irradiation, the sun energy density with a unit of J/m² or Wh/m² [1-3]. The component of solar irradiance is very important in the conversion of sunlight to electrical energy, using a PV module [4-6], which has a wide global application. This module is often applied in the DC application systems were observed according to [7-9], where their utilization in DC loads through the DC-DC converter. PV module is also commonly used in the AC application systems based on [10-13], where observation was conducted on their application in the pulse-width modulations (PWM) transformerless photovoltaic inverter (TPVI) system. These inverters were operated directly by a PV module, as the main DC energy source.

A wireless power transfer (WPT) system is an application of the electromagnetic concept used in transferring energy from a transmitter to a receiver coil (TC and RC) [14]. This system is constructed by a transmitter circuit, which converts DC to AC voltage source on the terminal of TC, through a half or full bridge inverter. It is also constructed by a receiver circuit, which obtains the AC voltage source on the RC as an electromagnetic linkage. Furthermore, the main energy of WPT is obtained from the DC voltage source, which needs to be converted to AC through an inverter circuit [15]. When the AC voltage source has a fixed frequency and supplies the main energy of this system, thus the LC tank should have similar parameters, due to being suitable for the connection and values of TC and RC capacitor and inductor. This shows that the capacitance and inductance values of the TC or RC capacitors and inductors need to be initially calculated on the LC tank, to meet the frequency of the AC voltage source. When this source is generated by a function generator and has varying frequencies, an adjustment should be subsequently performed according to the suitability of the LC tank. This explains that a suitable frequency is achieved when an electromagnetic field is generated, with the AC voltage being induced on the transmitter coil [16]. A DC voltage is also commonly applied to the WPT

system as the main power source. Based on the TC with and without center tap, the connection of the DC voltage source to the transmitter circuit is divided into two parts as follows, (a) The DC voltage source is connected directly to the switching driver circuit, which converts direct current to AC using a full bridge inverter. This is connected to the transmitter coil without a center tap [17], [18], [16], and (b) Two separate connections of DC voltage source are applied to the WPT's transmitter circuit. From these categories, the first connection of this power source is to supply the switching driver circuit, which converts DC to AC using a half-bridge inverter. This is subsequently connected to the transmitter coil without a center tap for its terminals. Meanwhile, the second connection shows the positive terminal of the DC voltage source is connected to the center terminal of the TC. It is also connected to the terminal connection of the transmitter circuit [19].

The common sources of DC voltage are batteries and various renewable energy, including fuel cells, wind power, and PV module. The PV module is a device that converts solar energy to DC electrical power, with its performance often depending on solar radiation and temperature. In this process, higher solar radiation leads to increased PV module performance, which is inversely proportional to the temperature. This indicates that increased temperature causes decreased PV module performance [20], [21]. To determine the most suitable area for the development of a PV module, the analysis of a solar radiation requirement is very important, especially for the DC voltage source of a WPT system, which transfers power from TC to RC (transmitter to receiver coil). In this system, the receiver coil is unable to be applied directly to 50 Hz AC loads, due to the WPT's utilization of high frequency until 100 kHz. This coil is connected to the rectifier circuit for conversion to a DC voltage source, which is only applied for small power loads [17], [18]. The operation of the WPT system also emphasizes an electromagnetic concept [22]. This is because the electromagnet generated is a function of periodic magnetic flux, indicating that the power transmitted and obtained by the transmitter and receiver coils are in AC form with a fixed frequency value. However, the pure sinusoidal waveform is unable to be reached in its application [23], due to

the TC and RC inductance being inappropriate or differently matched. This causes the power and efficiency on the receiver side of WPT are still low.

The WPT system is commonly constructed for a low-power system, due to the minimum energy of the selected switching components [24], [25]. This shows its inability to be applied to the high DC power source of the transmitter phase. It also has a near electromagnetic field range between the TC and RC, which causes low power and efficiency in the receiver phase. This indicates the need for a device, to increase the strength of the electromagnetic field on the straight radius center of the WPT system's transmitter and receiver coils. Therefore, this study aims to determine the effects of temperature and solar irradiance on the performance of the 50 Hz photovoltaic wireless power transfer (PVWPT) system. The DC main voltage source originates from the PV module and is converted to a 50 Hz AC waveform on the transmitter coil (TC), using an H-bridge circuit. The AC power is then transferred to the receiver coil (RC), using the electromagnetic field concept with the distance between the TC and RC. This is subsequently implemented using mutual inductance formulation. The effects of solar irradiance and temperature on the performance of the PVWPT system were also observed and analyzed with and without AC load.

2.0 METHODOLOGY

Figure 1(a) shows the block diagram of the proposed PVWPT system, which contains a PV module, a pulse driver circuit, an H-bridge inverter, a transmitter and receiver coil (TC and RC), an MRC (magnetic-relay coil), and an AC load. The PV module functions as a DC voltage source, which is converted to AC power.

The pulse driver circuit also emphasizes the production of 50 Hz waves, to drive the switching components on the H-bridge circuit. The conversion of the DC to AC voltage waveform on the TC is subsequently prioritized for the H-bridge circuit. Meanwhile, the TC, MRC, and RC transmits, help, and obtain the AC power, respectively, regarding the magnetic field concept.
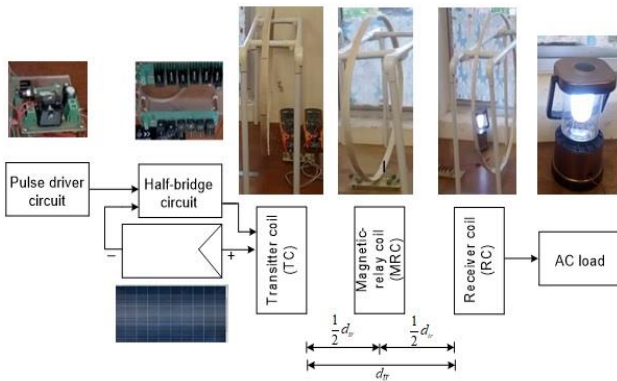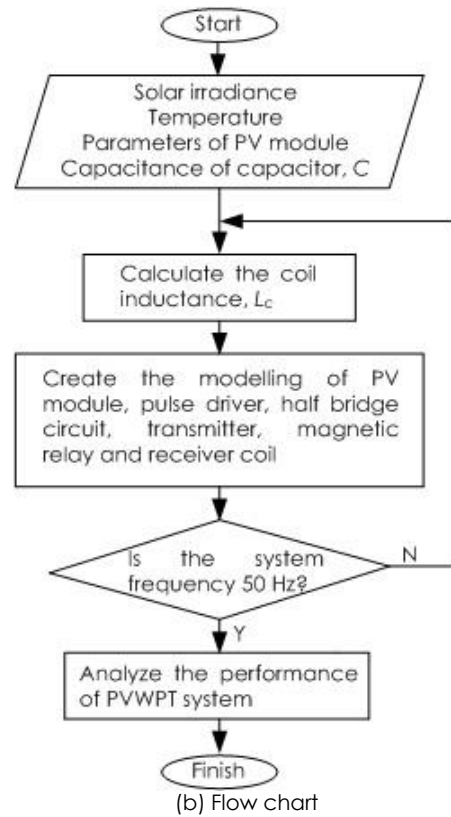

(a) Block diagram

(b) Flow chart

Figure 1 Block diagram and flow chart of 50 Hz proposed PVWPT system

Figure 1(b) shows the flow chart of the proposed PVWPT system. The data of solar irradiance and temperature are needed to operate the PV module with its specific parameter to generate the required voltage level. A value of capacitance of capacitor, C is decided to calculate the coil inductance, L_c for matching the system frequency of 50 Hz.

The PV module, pulse driver, half bridge circuit, transmitter, magnetic-relay and receiver coils are modelled using MATLAB-SIMULINK. The simulation results of AC voltage, current and power in the transmitter and receiver coils of PVWPT system are made to be sure to have the frequency of 50 Hz. The simulation results of PVWPT system performance are observed and analyzed, which they are related to the change of solar irradiance and temperature.

2.1 Modelling of PV Module

The modelling of PV module is needed as DC voltage source of PVWPT system. The input of PV module is solar irradiance and temperature, which affect the performance of PV module and PVWPT system.

The performance of PV module increases for the constant temperature and the higher solar irradiance, inversely it decreases for constant solar irradiance and the higher temperature. Also, these conditions will affect the performance of PVWPT system (the increasing of PV module performance will increase the performance of PVWPT system).

Table 1 Electrical parameter of PV module

Parameters	Value
Number cell per module	60
Maximum power (watt)	240
Open circuit voltage (volt)	37.5
Short circuit current (ampere)	8.75
Open circuit voltage at maximum power (volt)	29.3
Short circuit current at maximum power (ampere)	8.18
Temperature coefficient of open circuit voltage (%/°C)	-0.32
Temperature coefficient of short circuit current (%/°C)	0.05

A validation analysis was also conducted regarding the error percentage of the system's simulation and data sheet (Table 1). The results obtained were similar to the PV module performance in the curve analysis of current and power-voltage at the standard test condition (STC), where solar irradiance = 1000 W/m², temperature = 25°C and air pressure = 1 atm).

Based on Figure 2, the modelling process is constructed by a PV module and simple DC-DC converter block set from MATLAB-SIMULINK, using the electrical parameters presented in Table 1. These parameters are filled in the block data of the PV module.
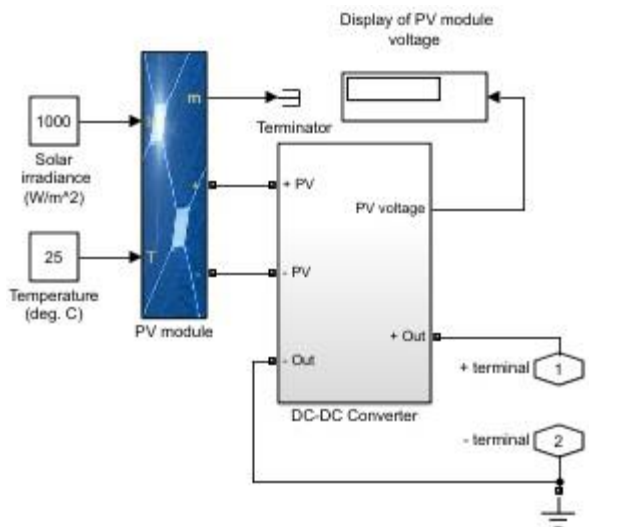
(a) PV module and DC-DC converter block set
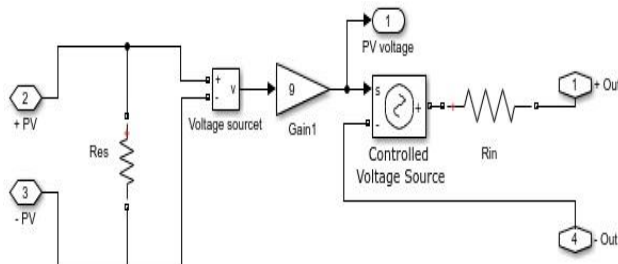
(b) Simple circuit of the DC-DC converter

Figure 2 Modeling of PV module as DC voltage source of PVWPT system

The simple circuit of the DC-DC converter was constructed by the following three main components, (1) The Resistor, which contains a R_{es} (estimated resistor) of 48 Ω, which is connected in parallel to adjust the suitable output voltage of the PV module. This component subsequently contains an input resistor (R_{in}) of 28 Ω, which is connected in series by the transmitter coil, to adjust the suitable AC voltage on the TC, MRC and RC, (2) A Gain Block, which indicates the number of series connection increasing the output voltage of PV module in one string process. In this case, nine modules were connected in series, where one open circuit voltage was 37.5 V. From this observation, the nine PV modules had a total voltage of 337.5 V. This was suitable for generating the AC voltage on the RC, with its peak or RMS values for a distance of 5 m between the TC and RC observed at 339 or 240 V, respectively, and (3) A Block of CVS (controlled voltage source), which is used for converting the SIMULINK input signal into an equivalent voltage source. In this case, positive and negative terminals are often obtained as representatives of the PV module.

2.2 Modelling of Pulse Driver and H-Bridge Circuit

Figure 3 shows the modelling of the pulse driver and H-bridge circuit. For the pulse driver, modelling was carried out through the block generator sets, S1 and S2, to produce a 50 Hz wave (Figure 4) and drive the Gate terminal of the MOSFETs, M1 and M2. These terminals were connected to the TC, due to the utilization of the H-bridge inverter. Therefore, the TC had a center tap connected to the positive terminal of the PV module, as shown in Figure 1.
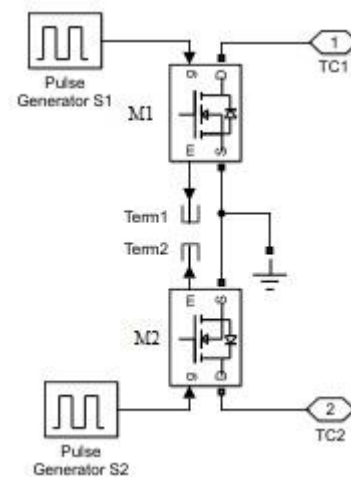

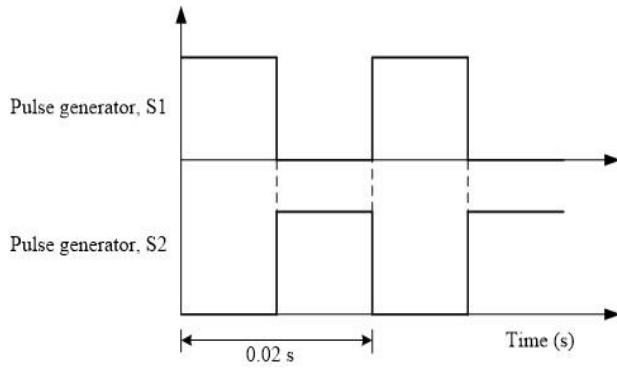**Figure 3** Modeling of pulse driver and H-bridge circuit

Figure 4 50 Hz pulse waves generated by the pulse generator

Based on Figure 4, the Gate terminals of M1 were driven by S1 for the first half cycle, with M2 observed to be OFF at the same time. Meanwhile, the terminal, M2 was driven by S2 for the second half cycle, with M1 found to be OFF during the process. These conditions generated an AC voltage on the TC.

2.3 Modelling of Transmitter, Magnetic-Relay and Receiver Coil

The TC, MRC and RC parameters were connected in parallel to a capacitor (C) and modelled to generate a 50 Hz AC voltage waveform. The inductance value (L_C) of these parameters was also obtained after determining a C-value (capacitor value) from the following Equation [1],

$$f = \frac{1}{2\pi}\sqrt{\frac{1}{L_c C}} \tag{1}$$

Figure 5 shows the modelling of TC, MRC and RC, where the values of the following were needed, (1) coil inductance, L_c, (2) coil resistance, R_c, and (3) mutual inductance, M. In this process, the solenoid coil was used, with its diameter (d_c), number of turns (N_c), and length (l_c) obtained through Equations (2) and (3). In addition, R_c was obtained using Equation (5) [2], [3].

$$d_c{}^2 N_c{}^2 - 40 d_w L_c N_c - 18 d_c L_c = 0 \tag{2}$$

$$l_c = \pi d_w N_c \tag{3}$$

$$A_w = \frac{1}{4}\pi d_w{}^2 \tag{4}$$

$$R_c = \rho\frac{l_c}{A_w} \tag{5}$$
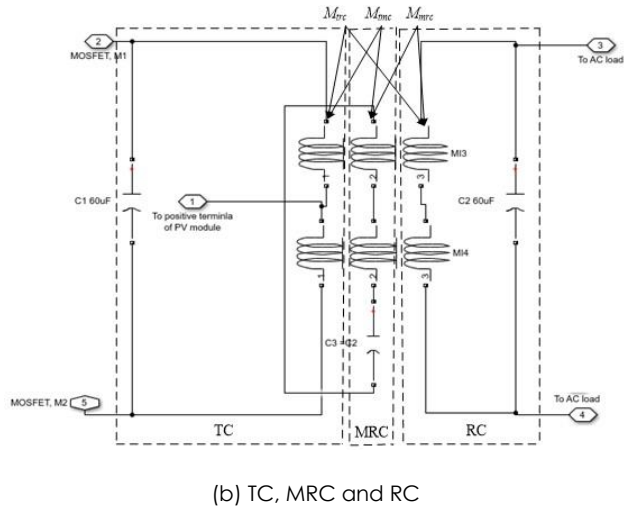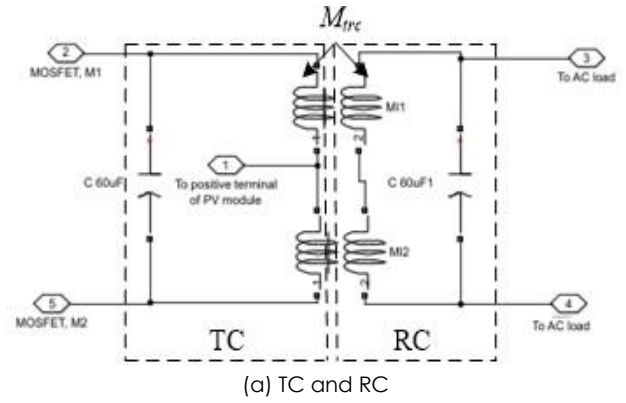

(a) TC and RC

(b) TC, MRC and RC

Figure 5 Modeling of the TC, MRC and RC

The TC and RC had a distance of d_{tr}, with the MRC positioned in the center of both coils (Figure 1). This indicated that the distance between TC/MRC or MRC/RC was $0.5d_{tr}$. Subsequently, this distance was represented by the following mutual inductance,

1. In Figure 5a, the distance between the TC and RC was d_{tr}, indicating that the mutual inductance between both coils (M_{tr}) was obtained from Equation (6) [4].

$$M_{trc} = \frac{\pi\mu_0 N_c{}^2 r_c{}^2 \text{x}10^{-2}}{\sqrt{\left(d_{tr}^2 + r_c^2\right)^3}} \tag{6}$$

where;
N_c = Turn number of coils (turn)
r_c = Radius of a coil (m)
d_{tr} = Distance between TC and RC (m)
M_{trc} = Mutual inductance between TC and RC (H)

2. Based on Figure 5b, the distance between the TC and RC was d_{tr}, showing that M_{tr} was obtained through Equation (6). In this case, the mutual inductances between the TC/MRC (M_{tmc}) and MRC/RC (M_{mrc}) were very similar, as shown in Equation (7).

$$M_{tmc} = M_{mrc} = \frac{\pi\mu_0 N_c^2 r_c^2 \times 10^{-2}}{\sqrt{\left((0.5d_{tr})^2 + r_c^2\right)^3}} \quad (7)$$

The total mutual inductance (M_t) was also obtained from Equation (8).

$$M_t = M_{trc} + M_{tmc} + M_{mrc} \quad (8)$$

2.4 Overall Modeling of PVWPT System

Figure 6 indicates the overall modelling of the PVWPT system, which was constructed by the PV module, pulse driver and H-bridge circuit, PT and RC, as well as R-load. In this process, an inductor of 100 µH was connected in series to the PV module and the center tap of the TC. The system also functioned as an AC

filter, to obtain a sinusoidal voltage waveform on the TC. This was conducted by combining the capacitor of 60 µF. Furthermore, the transmitter and receiver coils were transformed into TC, MRC, and RC (Figure 5b), to observe and analyze the effect of the magnetic relay coil on the performance of the PVWPT system.

Based on the simulation and analysis of the effects of solar irradiance, temperature and magnetic-relay coil on the performance of a 50-Hz PVWPT system, the validation of PV module modelling was initially carried out. This was conducted using error percentage, which is a comparative analysis of the module's simulation and datasheet. In this case, the simulation output is stated to be valid and applied as a DC voltage source to the PVWPT system when the error percentage is within ±10% [4].
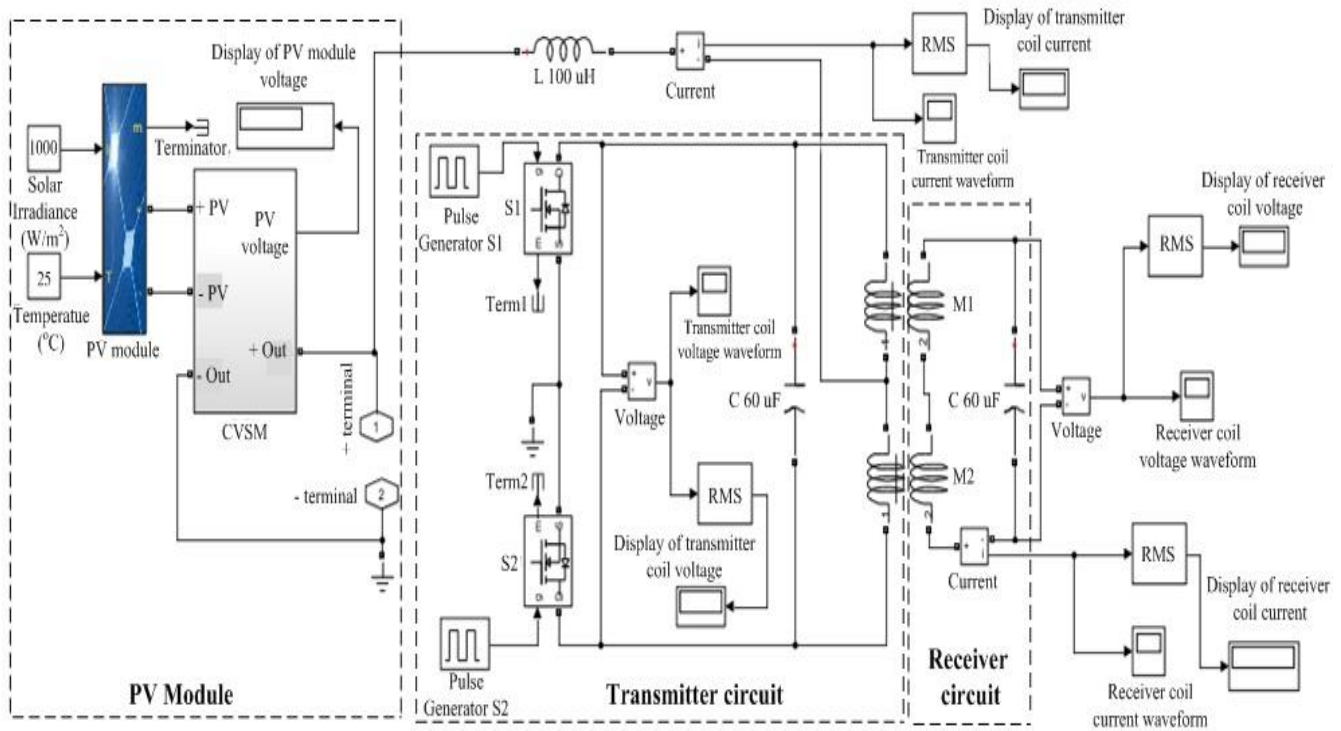
Figure 6 Overall modelling of the PVWPT system

This analysis is subsequently conducted through the 5 m distance between the TC and RC, with and without the MRC. The performances of PVWPT system emphasized the AC voltage, current, and active power on the TC and RC. Moreover, both coils were more characteristically inductive, although had a few resistive features. This proved that active power (AP) was still generated by the TC and RC. In this case, AP was considered a power factor, which was obtained by observing the AC voltage and current on the transmitter and receiver coils. This confirmed that the active power on both coils was calculated using Equations (9) and (10). The efficiency of PVWPT, η, is observed through Equation (11).

$$P_{tc} = I_{tc} \times V_{tc} \times \cos\theta \quad (9)$$
where,
P_{tc} = Active power on the TC (W)
I_{tc} = RMS AC current on the TC (A)
V_{tc} = RMS AC voltage on the TC (V)
$\cos\theta$ = power factor

$$P_{rc} = I_{rc} \times V_{rc} \times \cos\theta \quad (10)$$
where,
P_{rc} = Active power on the RC (W)
I_{rc} = RMS AC current on the RC (A)
V_{rc} = RMS AC voltage on the RC (V)

$$\eta = \frac{P_{rc}}{P_{tc}} \times 100\% \qquad (11)$$

Based on these equations, a maximum resistive load was connected to the RC, regarding the active power obtained for the solar irradiance, temperature, and distance of 1000 W, 25°C and 5 m, respectively. The performances of PVWPT system were also observed and analyzed for varying solar irradiance and temperature, with and without the MRC.

3.0   RESULT AND DISCUSSION

The PV module performances were simulated and analyzed using the solar irradiance and temperature of 1000 W/m² and 25°C, respectively. The results obtained were also validated using error percentage, with the system's performance presented in the curve of current and power-voltage. Based on the analysis, the PV module connected in series had an open circuit voltage of 37.5 V, indicating that nine connections produced a total of 337.5 V. This was subsequently supplied to the AC voltage on the TC and RC of the PVWPT system. The AC voltage waveform generated on the TC was also observed and analyzed, to prove a system frequency of 50 Hz for the solar irradiance and temperature of 1000 W/m² and 25°C, respectively. Using the electromagnetic field concept, the AC waveform was transferred from the TC to the RC. This waveform was subsequently produced on the receiver coil and used as the voltage source of the AC loads.

The effects of solar irradiance and temperature on the performance of the PVWPT system were also analyzed, with the voltage, current, PV module power, TC, and RC emphasized in the 3-D dimension graph as functional parameters. In addition, the efficiency of this system was analyzed as a comparison between the TC and RC power in no AC load condition, using a distance of 5 m. Based on the results, a resistive load of 100 W was connected to the receiver coil, where the AC voltage, current and power were appropriately analyzed. Subsequent analysis was also carried out for the constant temperature and solar irradiance of 25°C and 1000 W/m², as well as other related parameters.

3.1 Validation of PV Module

Using the curves of current and power-voltage, the PV module performances were simulated to ensure the validity of the proposed system as a DC source. In this case, the results obtained were also compared to the system's data sheet. Figure 7 shows the curves of current and power-voltage, which were simulated at the solar irradiance and temperature of 1000 W/m² and 25°C in the standard test conditions (STC).

From the results, the short-circuit current and open-circuit voltage of the PV module were 8.75 A and 37.5 V for each simulation (Figure 7) and data sheet (Table 1), respectively. This indicated an error percentage of

0% for both comparative analyses. Moreover, the maximum power values of the module were 239.7 W and 240 W for the simulation and data sheet, respectively. This confirmed an error percentage of -0.125%, where the simulation output was lower than the data sheet of the system. Regarding the error percentages within ±10%, the simulation outputs of PV module performances were valid and applied as the DC voltage source of the PVWPT system.
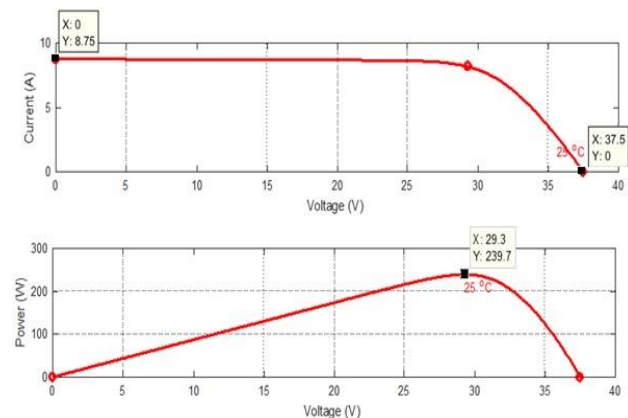

Figure 7 Current versus voltage and power versus voltage of PV module

Based on the open-circuit voltage of 37.5 V, nine PV modules were connected in series to generate a total of 337.5 V. This validated DC source was then converted to the AC voltage on the TC, using an H-bridge circuit. Figure 8 shows the output and input voltages of the DC-DC converter from the nine modules connected in series. For the solar irradiance and temperature of 1000 W/m² and 25°C, the output voltage of this converter was 332.9 V in the loaded condition to the PVWPT system. This indicated a decrease of 4.6 V, due to a voltage across the input resistor, R_{in}, (Figure 2b). Irrespective of the drop, the DC-DC converter's output voltage (332.9 V) still performed to supply the PVWPT system. This possessed a stable DC voltage source during the operation of the system.
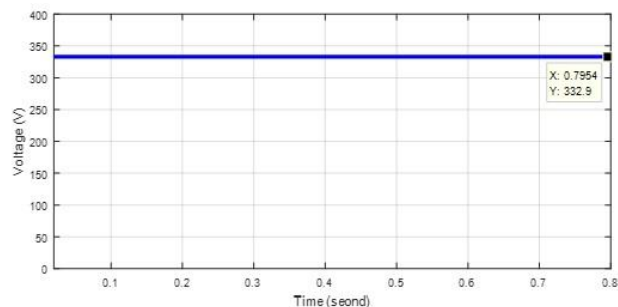

Figure 8 Output voltage of nine PV modules in series connection

Figure 9 shows the output current of the nine PV modules in series connection, for the solar irradiance and temperature of 1000 W/m² and 25°C, respectively. In this process, the modules produced an output current of 8.18 A, although only 6.61 A was utilized by the DC-DC converter. This was because 1.57 A had split into the controlled voltage source (Figure 2b). Irrespective of this split, the output current of 6.61 A was still stable and supplied to the PVWPT system.
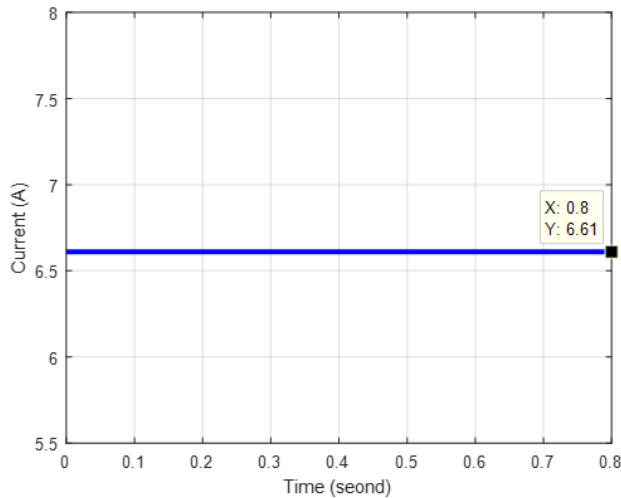

Figure 9 Output current of nine PV modules in series connection

3.2 AC Voltage Waveforms on The TC and RC

Based on Figure 6, the positive and negative terminals of the DC-DC converter's output voltage (332.9 V) were supplied and connected to the TC center tap and MOSFETs Source point, respectively. Using the H-bridge circuit, this DC voltage, 332.9 V, was then converted to an AC waveform, as shown in Figure 10. The sinusoidal form of these AC voltage waveforms was due to the effect of the 60 µF capacitor connected in parallel to the TC. It was also because of the 100 µH inductors connected in series to the center tap of the TC.

From Equation (1), the inductor value (L_C) of TC and RC was 0.17 H for the capacitor (c) and system frequency (f) of 60 µF and 50 Hz, respectively. The transmitter and receiver coils were also simulated using coated magnet copper (CMC) wire with d_w (wire diameter), ρ (resistivity), and d_c (coil diameter) of 0.05 in/1.27 mm, 1.68x10⁻⁸ Ωm, and 78.74 in/2 m, respectively. In this process, the turn number of each coil was 226 turns, according to Equation (2). Based on Equations (3) to (5), the resistance of each coil, R_C, was also 18.80 Ω. Since the distance of TC and RC (d_{tr}) = 5 m, the mutual inductance, M_{trc}, was subsequently observed as 0.154 H (Equation 6). Therefore, the L_C, R_C, and M_{trc} of 0.17 H, 18.80 Ω, and 0.154 H, were filled in the TC and RC (Figure 5), respectively, to obtain the

AC voltage waveforms (Figure 10) with a system frequency (*f*) of 50 Hz.
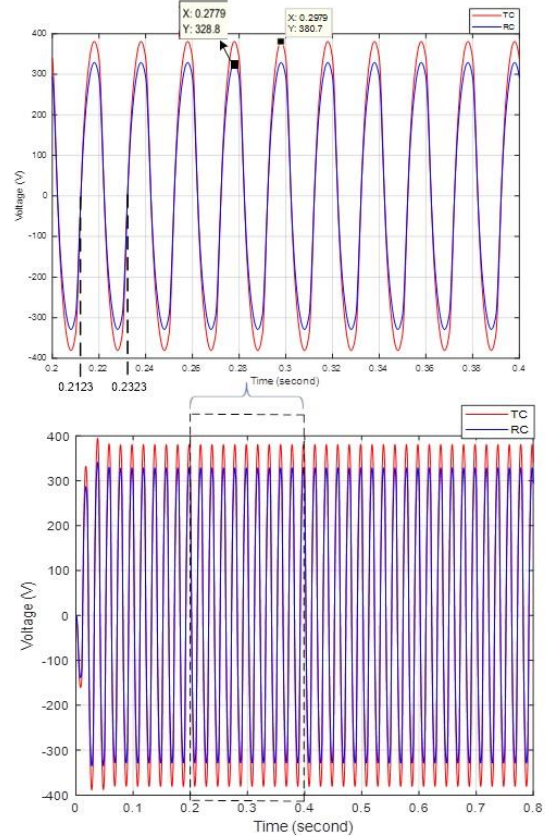

Figure 10 AC voltage waveform on the TC and RC for the distance of 5 m

Based on Figure 10, the PVWPT system was operated at the solar irradiance and temperature of 1000 W/m² and 25°C, respectively. This was to generate the DC-DC converter's output voltage terminal of 332.9 V at a 5-metre distance for TC and RC. It was also used to generate the peak/RMS AC voltage of 380.7/269.2 V on the TC, with 328.8/232.5 V observed on the RC. The time observation of 0.2123-0.2323 s also showed that the period or frequency of the AC waveforms on TC and RC was 0.02 s or 50 Hz, respectively. For the RC, the AC voltage was similar to the load source at 232.5 V and 50 Hz. This indicated that the receiver coil was suitable for application on the AC loads with rated voltage and frequency of 240 V and 50 Hz, respectively, due to its existence in the allowed utilization range (240 V -10% to 240 V +5% = 216 V to 252 V) [6].

3.3 Effect of Temperature and Solar Irradiance on The Performance of PVWPT System

The solar irradiance and temperature affected the performance of the PV module, regarding its voltage, current, and power [4]. The performance transformation also influenced the efficiency of the PVWPT system, due to the main DC source originating

from the PV module, which depended on solar irradiance and temperature.

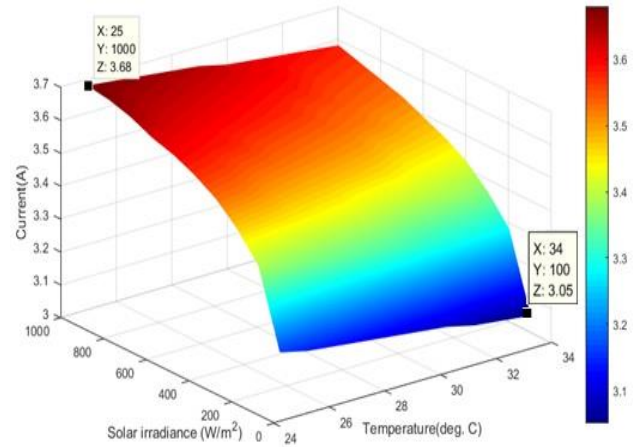Figure 11 shows the effect of solar irradiance and temperature on the PV module performance in a 3D-dimension graph. At the solar irradiance and temperature of 100 W/m^2 and 34°C, the lowest values of PV module voltage, current and power were 275.7 V, 5.49 A, and 1514 W, respectively. Meanwhile, the highest values of voltage, current and power were 332.9 V, 6.63 A, and 2207 W at 1000 W/m^2 and 25°C, respectively. Based on these results, the PV module performance for current, voltage and power increased with the constant temperature and the increasing solar irradiance. This performance however decreased with the constant solar irradiance and the increasing temperature.
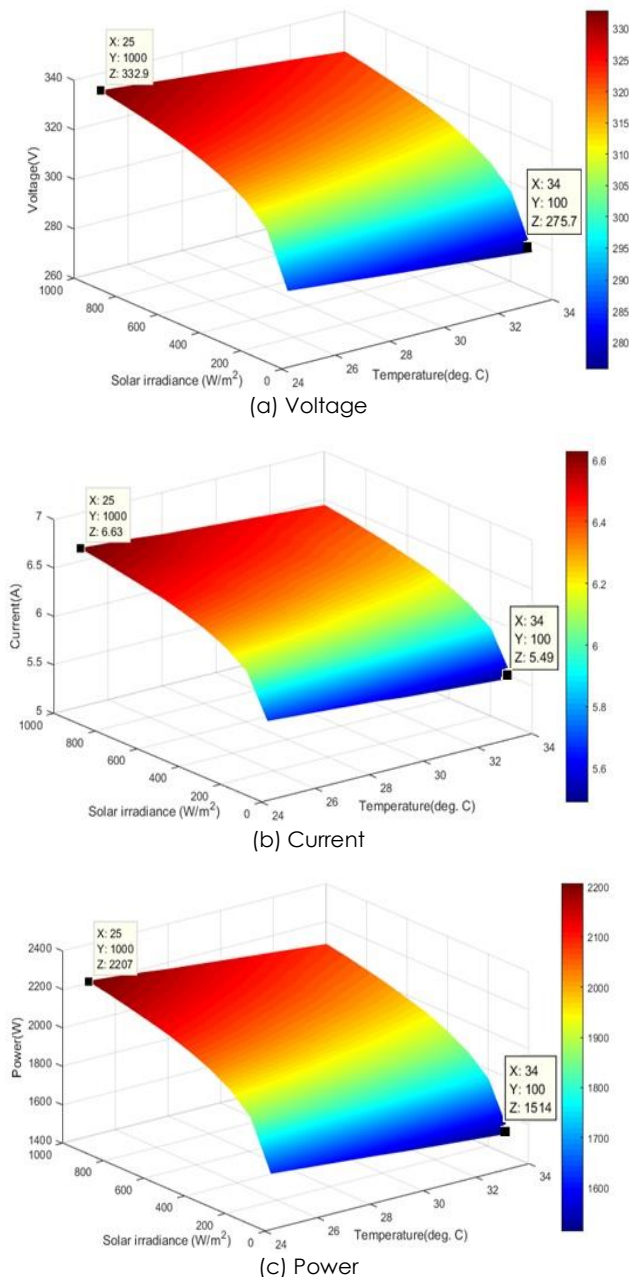
From the results, the AC voltage was generated on the TC, where its RMS value depended on the output voltage of the DC-DC converter. This was due to the closed-loop systematic relationship between the L_c and C in parallel connection, leading to an AC current flow and power generation through the coil inductor and on the TC, respectively. Figure 12 shows the effect of solar irradiance and temperature on the TC performance (voltage and power) in a 3D-dimension graph. At the solar irradiance and temperature of 100 W/m^2 and 34°C, the lowest values of TC voltage and power were 222.9 V and 1224 W, respectively. Meanwhile, the highest values of voltage and power were 269.2 V and 1785 W at 1000 W/m^2 and a temperature of 25°C. Based on these results, the TC performance for voltage and power increased with the constant temperature and the increasing solar irradiance. This performance however decreased with the constant solar irradiance and the increasing temperature.

From these results, the electromagnetic field generated by the TC reached the RC at a distance of 5 m, leading to the generation of an AC voltage on the coil. This was due to the closed-loop systematic relationship between the L_c and C, causing an AC current flow and power generation on the RC. In addition, this power generation depended on the following, (1) The AC voltage and current, (2) The electromagnetic field, (3) The AC voltage on the TC, and (4) The PV module performance. Figure 13 shows the RC performance in a 3D-dimension graph, as a function of the solar irradiance and temperature at a 5-metre distance.
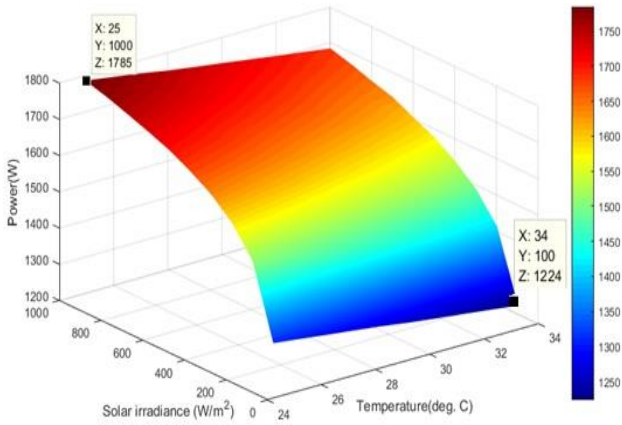
At the solar irradiance and temperature of 100 W/m^2 and 34°C, the lowest values of RC voltage, current, and power were 192.6 V, 3.05 A, and 587.4 W, respectively. However, the highest values of RC voltage, current and power were 232.5 V, 3.68 A, and 855.6 W at 1000 W/m^2 and 25°C, respectively. Based on these results, the RC performance for current, voltage, and power increased with the constant temperature and increasing solar irradiance. This performance however decreased with the constant solar irradiance and the increasing temperature.
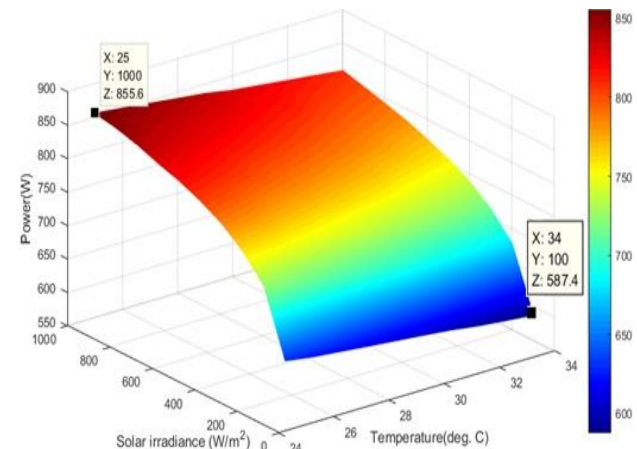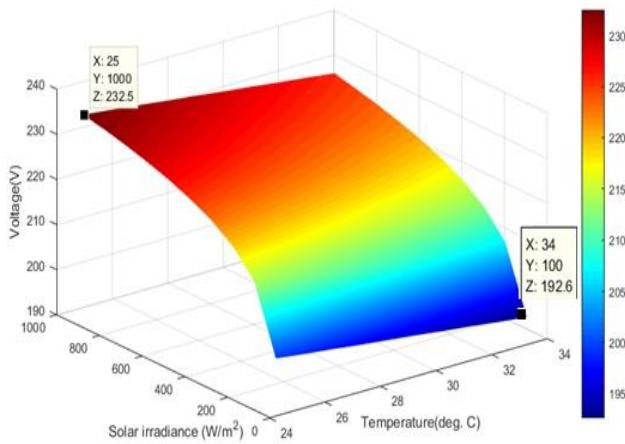

(a) Voltage

(b) Current

(c) Power

Figure 11 Effect of solar irradiance and temperature on the PV module performance
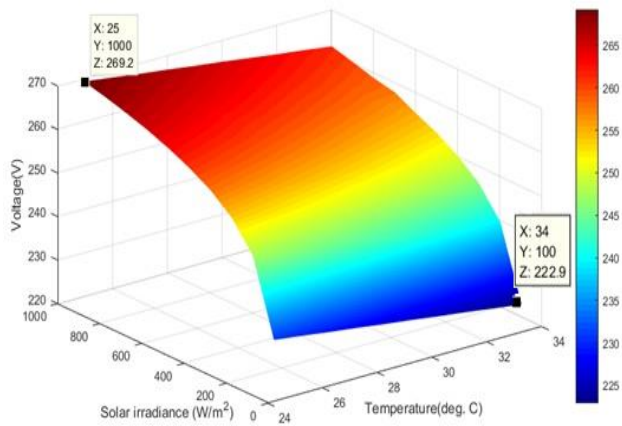
(a) Voltage

(b) current

(b) Power

Figure 12 Effect of solar irradiance and temperature on the TC performance

(c) Power

Figure 13 Effect of solar irradiance and temperature on the RC performance

(a) Voltage

From Figures 12b and 13c, the PVWPT system was found to transfer AC power to the transmitter and receiver coils at a distance of 5 m, respectively. This led to the comparative analysis of the power transferred to these coils, to observe the efficiency of the system. Figure 14 shows the efficiency of the PVWPT system in a 3D-dimension graph, as a function/effect of the solar irradiance and temperature. This showed that the relationship of AC power on TC and RC was proportional, indicating synergistic conditions for both coils. For instance, high TC power leads to increased RC energy and vice versa. The results also confirmed that the PVWPT system needs to have similar efficiency for the transformation of solar irradiance and temperature, as well as a fixed distance of 5 m. Irrespective of these conditions, an efficiency difference was still observed in the experimental range provided. At the solar irradiance and temperature of 100 W/m^2 and 26°C, the lowest value of PVWPT efficiency was 47.92%. Meanwhile, the highest value was 48.1% at 1000 W/m^2 and 29°C. This proved that the efficiency of the PVWPT

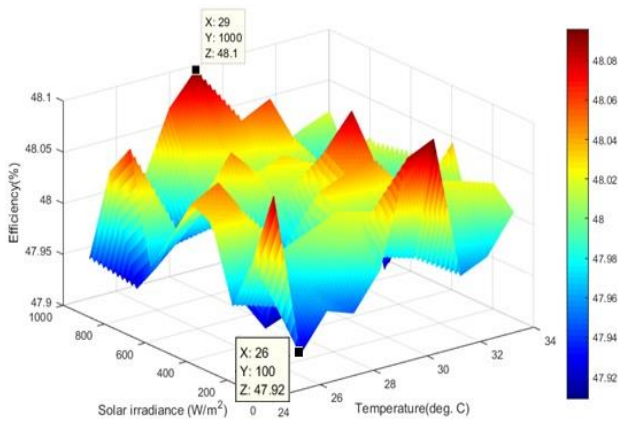system ranged from 47.92-48.1%, with its average value being 48%.

Figure 14 Effect of solar irradiance and temperature on the efficiency
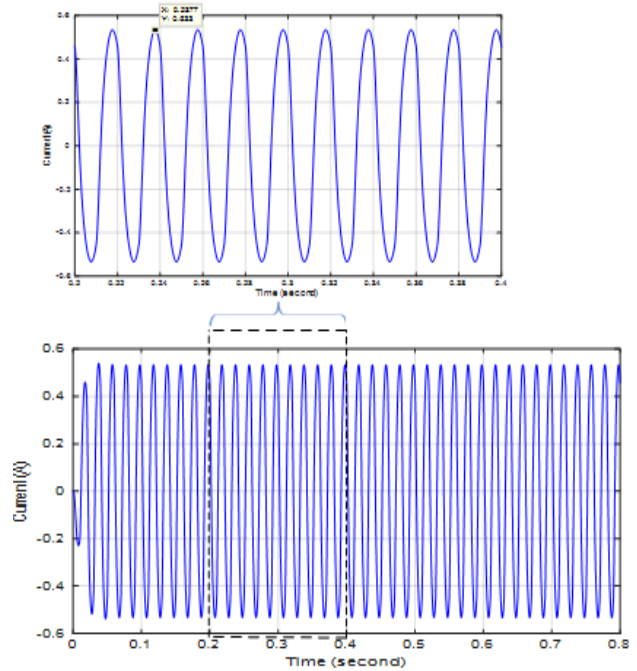
3.4 Performance of The PVWPT System in AC Load Condition

For various temperature and solar irradiance of 25-34°C and 100-1000 W/m², RC had a system frequency and AC power capacity of 50 Hz and 587.4-855.6 W, respectively, as an AC voltage source. This proved that AC voltage and current were observed and analyzed when an AC load of 100 W was connected to the RC at the solar irradiance and temperature of 1000 W/m² and 25°C, respectively.

Figure 15 shows the AC load voltage and current at 1000 W/m² and 25°C. In this process, the RMS AC load voltage and current were 217.5 V and 0.377 A, respectively. This indicated that 217.5 V still met the standard of ANSI C84.1 2016, concerning the utilization of AC voltage [16]. However, no AC load condition was observed for the AC voltage of RC at 1000 W/m² and 25°C, regarding the comparative analysis, conducted. From this result, a drop of 15 V was observed, as the AC voltage decreased from 232.5 V to 217.5. This was due to the availability of the fixed electromagnetic field produced by the TC, which did not change with the AC loads' transformation.
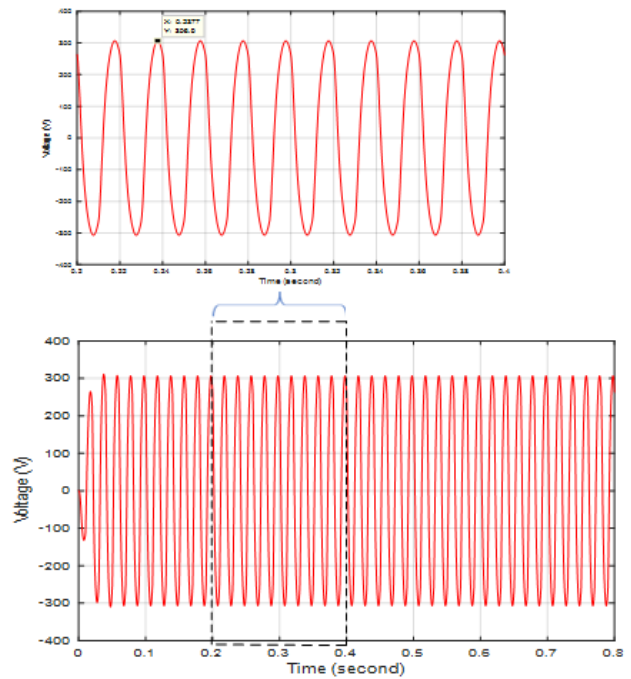

(a) AC load voltage waveform

(a) AC load current waveform

Figure 15 AC load performance at solar irradiance of 1000 W/m² and temperature of 25°C
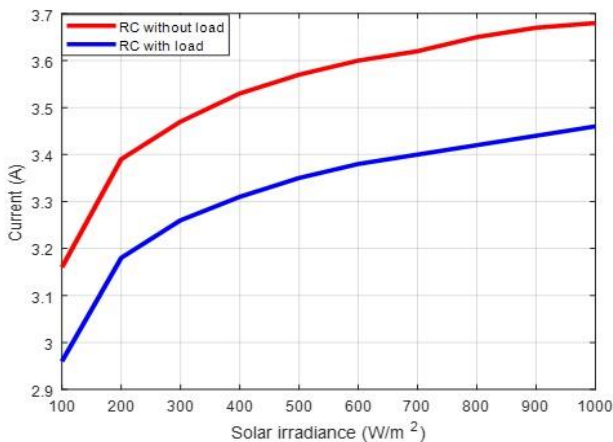
3.4.1 Constant Temperature of 25°C and Various Solar Irradiance

A simulation of the PVWPT system was also conducted in 0 and 100 W AC load conditions, at the constant temperature of 25°C and various solar irradiance. In this process, the performances of RC and AC load determined the change effect of solar irradiance for the constant temperature. Figure 16 shows the change effect of solar irradiance on the RC performance, with and without the AC load. This indicated that the receiver coil performance for voltage, current, and power increased through the elevation and maintenance of solar irradiance and fixed temperature.

When the RC was connected to the AC load, a voltage drop was observed (Figure 16a). In this case, the elevation of solar irradiance led to the higher AC voltage of RC. When compared to the coil's AC voltage without load, the average reduction difference was 15 V. Similar conditions were found for the AC current and power flowing through the RC (Figures 16b and 16c), which increased by elevating the solar irradiance.
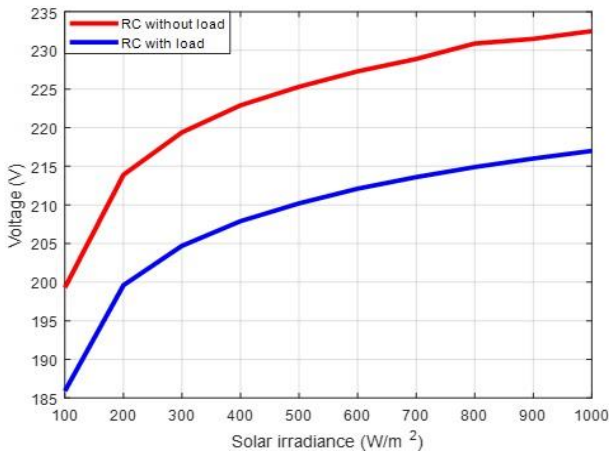

(a) AC voltage

(b) AC current
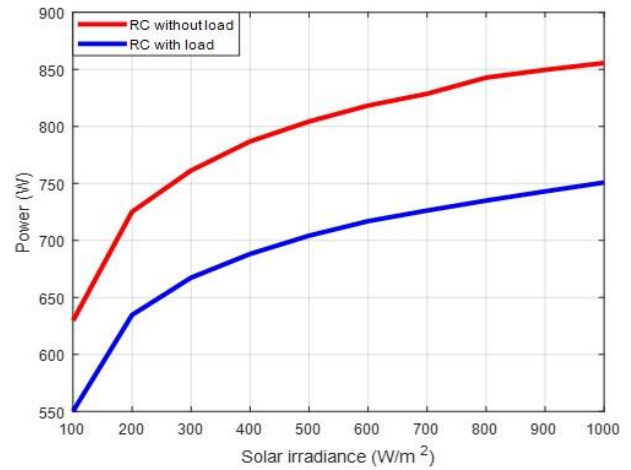
(c) AC power

Figure 16 The performance of RC for a constant temperature of 25°C and various solar irradiance

Figure 17 shows that the AC load condition for current and power performance supported the change in solar irradiance. However, the condition remained unchanged for the RC with load, regarding voltage performance (Figure 16a). Based on the results, the elevation of solar irradiance led to higher AC load current and power. In this case, the power did not reach 100 W, indicating that only 81.81 W was observed. Irrespective of this condition, the solar irradiance was still found at approximately 1000 W. This was because the electromagnetic field generated by the TC did not support the generation of the AC voltage on the RC, regarding the supply of the load.
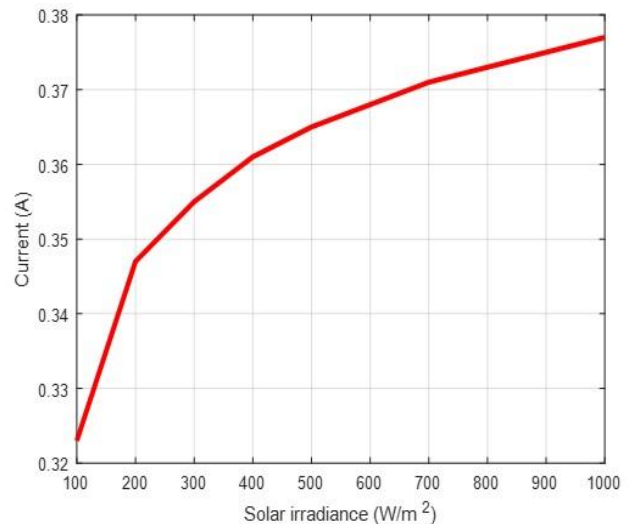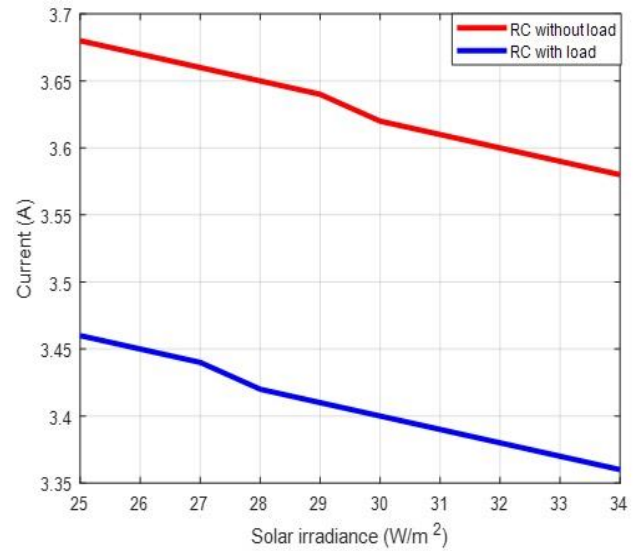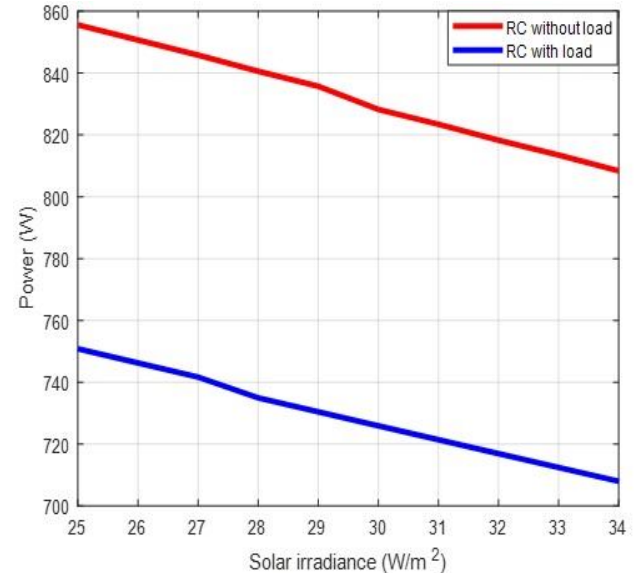

(a) AC load current
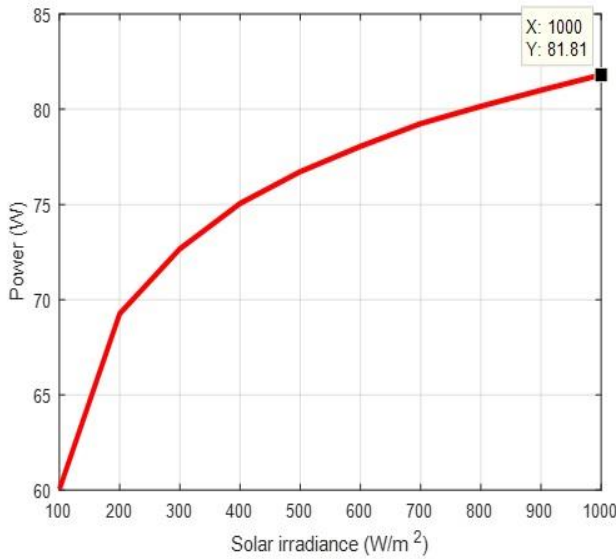
(b) AC load power

Figure 17 AC load performance for constant temperature of 25°C and various solar irradiance

3.4.2   Constant Solar Irradiance of 1000 W/m² and Various Temperature

In AC load conditions, the PVWPT system was simulated for the constant solar irradiance of 1000 W/m2 and various temperatures. This showed that the continuous elevation of temperature led to decrease PV module performance, which then negatively affected the efficiency of the PVWPT system. In Figure 18, the performance of RC was observed for constant solar irradiance and various temperature. This indicated that the AC voltage, current, and power of RC decreased with increasing systematic temperature, with and without load.
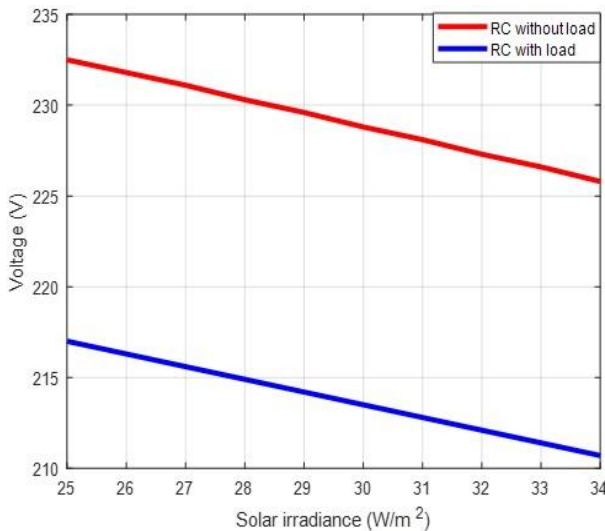

(a) AC voltage

(b) AC current

(c) AC power
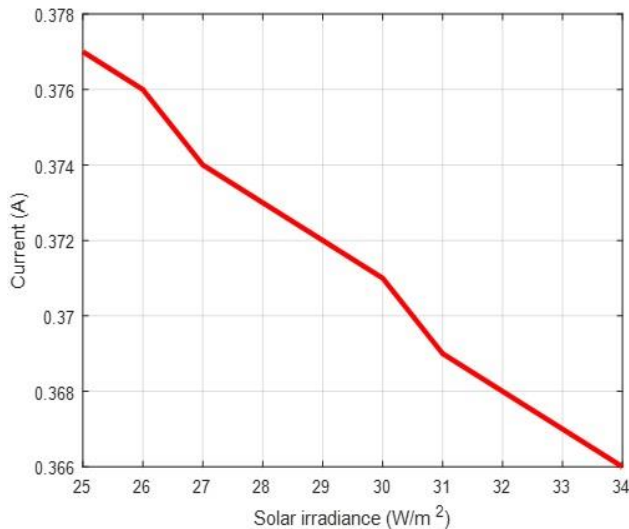
Figure 18 The performance of RC for constant solar irradiance and various temperature
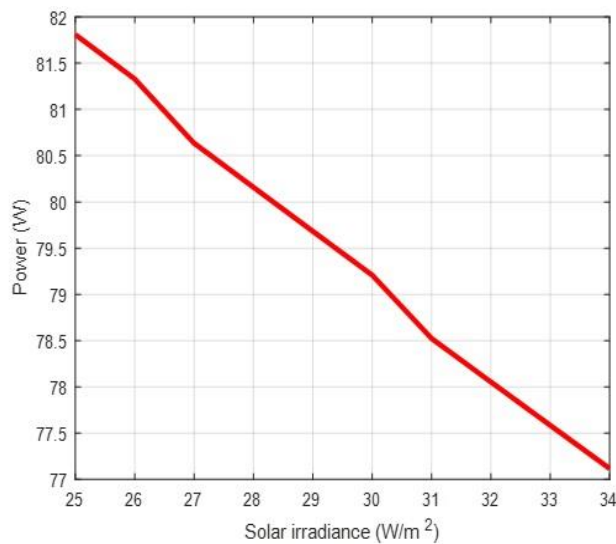
Figure 19 presents the AC load condition of current and power performance, for constant solar irradiance and various temperature. In this case, the AC load voltage remained unchanged for the RC with a load. This proved that temperature elevation led to decreased AC load voltage, current, and power.

(a) AC load current

(b) AC load power

Figure 19 AC load performance for constant solar irradiance and various temperature

4.0 CONCLUSION

A PVWPT system was modelled and simulated to generate an AC voltage waveform on the transmitter coil (TC). This was then transferred to the RC for AC load performance, regarding the electromagnetic field concept. The PVWPT system was supplied by some PV modules in series connection, to generate a higher DC voltage. The PV module simulation results for short-circuit current and open-circuit voltage were 8.75 A and 37.5 V. This indicated an error percentage of 0% for both comparative analyses. Regarding the error percentages within ±10%, the simulation outputs of PV module performances were valid and applied as the DC voltage source of the PVWPT system.

The PV module performance depended on solar irradiance and temperature. In this case, increasing solar irradiance and temperature led to higher and lower PV module and PVWPT system performance, respectively. For the solar irradiance at 1000 W/m² and temperature at 25°C, the RMS AC load voltage and current of PVWPT system were 217.5 V and 0.377 A, respectively. This indicated that 217.5 V still met the standard of ANSI C84.1 2016, concerning the utilization of AC voltage.

For the distance, as well as various temperatures and solar irradiance of 5m, 25-34°C, and 100-1000 W/m², respectively, the average efficiency of the PVWPT system was 48%.

Acknowledgement

References

[1] M. Irwanto, H. Alam, M. Masri, B. Ismail, Z. Leow and Y. M. Irwan. 2019. Solar Energy Density Estimation Using ANFIS Based on Daily Maximum and Minimum Temperature. *International Journal of Power Electronics and Drive System (IJPEDS)*. 10(4): 2206-2213. Doi: 10.11591/ijpeds.v10.i4.2206-2213.

[2] R. Gallo, M. Castangia, A. Macii, E. Macii, E. Patti and A. Aliberti. 2022. Solar Radiation Forecasting with Deep Learning Techniques Integrating Geostationary Satellite Images. *Engineering Applications of Artificial Intelligence*. 116: 105493. Doi: doi.org/10.1016/j.engappai.2022.105493.

[3] S. Zhao, L. Wu, Y. Xiang, J. Dong, Z. Li, X. Liu, Z. Tang, H. Wang, X. Wang, J. An, F. Zhang and Z. Li. 2022. Coupling Meteorological Stations Data and Satellite Data for Prediction of Global Solar Radiation with Machine Learning Models. *Renewable Energy*. 198: 1049-1064. Doi: doi.org/10.1016/j.renene.2022.08.111.

[4] M. Irwanto, W. Z. Leow, B. Ismail, N. H. Baharudin, R. Juliangga, H. Alam and M. Masri. 2020. Photovoltaic Powered DC-DC Boost Converter Based on PID Controller for Battery Charging System. *Journal of Physics: Conference Series*. 1432: 012055. Doi: 10.1088/1742-6596/1432/1/012055.

[5] L. Micheli, D. L. Talavera, G. M. Tina, F. Almonacid, E. F. Fernandez´. 2022. Techno-Economic Potential and Perspectives of Floating Photovoltaics in Europe. *Solar Energy*. 243: 203-214. Doi: doi.org/10.1016/j.solener.2022.07.042.

[6] Y. Haozhe, Y. Huanhuan, C. Yaoting, D. Wenyang. 2022. Research on the Optimal Confguration of Photovoltaic and Energy Storage in Rural Microgrid. *Energy Reports*. 8: 1285-1293. Doi: doi.org/10.1016/j.egyr.2022.08.115.

[7] M. Irwanto, T. A. Taha, A. T. Hussain, M. Masri and H. Alamz. 2018. Hybrid Charger Controller Based PV and Wind Turbine Systems. *International Journal of Research in Advanced Engineering and Technology*. 4(2): 73-77.

[8] M. Dhimish and N. Schofield. 2022. Single-switch Boost-buck DC-DC Converter for Industrial Fuel Cell and Photovoltaics Applications. *International Journal of Hydrogene Energy*. 47: 1241-1255. Doi: doi.org/10.1016/j.ijhydene.2021.10.097.

[9] A. Raj, R. P. Praveen. 2022. Highly Efficient DC-DC Boost Converter Implemented with Improved

MPPT Algorithm for Utility Level Photovoltaic Applications. *Ain Shams Engineering Journal.* 13: 101617. Doi: doi.org/10.1016/j.asej.2021.10.012.

[10] H. Alam, M. Irwanto, Y. M. Mashor and M. Masri. 2020. Design of Multiple Pulse Width Modulation (MPWM) Transformerless Photovoltaic Inverter (TPVI) System. *Journal of Physics: Conference Series.* 1432: 012056. Doi: 10.1088/1742-6596/1432/1/012056.

[11] M. Mohan, J. Joy, G. James and S. Paulose. 2022. Switched Inductor based Transformerless Boost Inverter. *Materials Today: Proceedings.* 58: 496-503. Doi: doi.org/10.1016/j.matpr.2022.03.010.

[12] S. Kraiem, M. Hamouda and J. B. H. Slama. 2022. Conducted EMI Mitigation in Transformerless PV Inverters Based on Intrinsic MOSFET Parameters. *Microelectronics Reliability.* 114: 113876. Doi: doi.org/10.1016/j.microrel.2020.113876.

[13] Z. Liao, C. Cao, D. Qiu. 2019. Analysis on Topology Derivation of Single-Phase Transformerless Photovoltaic Grid-Connect Inverters. *Optik - International Journal for Light and Electron Optics.* 182: 50-57. Doi: doi.org/10.1016/j.ijleo.2018.12.169.

[14] A. H. Butar-Butar, J. H. Leong, M. Irwanto, A. H. Haziah, M. Masri and A. Alam. 2018. Simulation of Magnetic Density Field in Solenoid Generated by Current of Photovoltaic Module Based on Solar Irradiance and Temperature. *Far East Journal of Electronics and Communications.* 17(5): 1285-1298. Doi.org/10.17654/EC017051285.

[15] A. H. Butar-Butar, J. H. Leong, M. Irwanto. 2020. Effect of DC Voltage Source on the Voltage and Current of Transmitter and Receiver Coil of 2.5 kHz Wireless Power Transfer. *Bulletin of Electrical Engineering and Informatics.* 9(2): 484-491. Doi: 10.11591/eei.v9i2.2060.

[16] D. B. Surajit, W. R. Ahmed, K. Narendra, K. Md. Ershadul and & B. M. Abu. 2015. Wireless Powering by Magnetic Resonant Coupling: Recent Trends in Wireless Power Transfer System and Its Applications. *Renewable and Sustainable Energy Reviews.* 51: 1525-1552.

[17] G. D. Capua, N. Femia and G. Lisi. 2016. Impact of Losses and Mismatches on Power and Efficiency of Wireless Power Transfer Systems with Controlled Secondary-side Rectifier, INTEGRATION. *The VLSI Journal.* 55: 384-392.

[18] S. Chattaerjee, A. Iyer, C. Bharatiraja, I. Vaghasia and V. Rajesh. 2017. Design Optimisation for an Efficient Wireless Power Transfer System for Electric Vehicle. *1st International Conference on Power Engineering, Computing and Control.* PECON-2017, 2-4 March, VIT University, Chennai Campus.

[19] M. Iordache, G. Andronescu, V. Bucata, M. L. Iordache, M. Staculescu and D. Nuculae. 2016. Design and Simulation of Wireless Power Transfer Systems. *Annals of the University of Craiova, Electrical Engineering Series.* 20: 109-114.

[20] K. Saleh, M. Irwanto, A. H. Haziah, H. Alam and M. Masri, M. 2017. Estimation of Solar Irradiation in Medan using Hargreaves method Based on Minimum and Maximum Temperature for Potential Assessment of Photovoltaic Power Generation. *Advanced Science Letters.* 23(5): 4463-4466,

[21] A. Nuwolo, M. Irwanto, A. H. Haziah and A. Kusmantoro. 2017. Estimation of Clear Sky Global Solar Irradiance as Potential of Electrical Power Generation of Photovoltaic Module Based on Latitude Angle in Semarang, Indonesia. *International Journal of Research in Advanced Engineering and Technology.* 3(1): 41-45.

[22] Y. Wang, J. Qiao, J. Du, F. Wang and W. Zhang. 2018. A View of Research on Wireless Power Transfer. *IOP Conf. Series: Journal of Physic: Conf. Series.* 1074: 1-7.

[23] X. Wang, X. Nie, Y. Liang, F. Lu, Z. Yan and Y. Wang. 2017. Analysis and Experimental Study of Wireless Power Transfer with HTS Coil and Copper Coil as the Intermediate Resonators System. *Physica C: Superconductivity and Its Applications.* 532: 6-12.

[24] L. Aravind and P. Usha 2015. Wireless Power Transmission using Class E Power Amplifier from Solar Input. *Inter. J. Engin. Res. Tech. (IJERT).* 4(06): 390-395.

[25] A. A. Eteng, S. K. A. Rahima, C. Y. Leowa, S. Jayaprakasama and B. W. Chew. 2017. Low Power Near-Field Magnetic Wireless Energy Transfer Links: A Review of Architectures and Design Approaches. *Renewable and Sustainable Energy Reviews* 72: 486-505.